https://doi.org/10.5194/egusphere-2023-2183
Preprint. Discussion started: 16 November 2023

The characteristics of cloud macro parameters caused by seeder-feeder inside clouds measured by millimeter-wave cloud radar in Xi'an

Huige Di*, Yun Yuan

School of Mechanical and Precision Instrument Engineering, Xi'an University of Technology, Xi'an 710048, China

* Corresponding author: dihuige@xaut.edu.cn

Abstract

The seeding effect of upper clouds on lower clouds affects the evolution of clouds, especially the seeding from upper ice clouds on lower stratiform clouds or convective clouds, which can stimulate the precipitation of lower clouds and even produce extreme precipitation. Because when seeders of seeding cloud enter the feeding cloud, the interaction between cloud particles results in the change of macro and micro parameters of the feeding cloud. Based on the observation data of the ground-based Ka-band millimeter-wave cloud radar (MMCR) and microwave radiometer (MWR) in spring and autumn from 2020 to 2022, the seeder-feeder phenomenon among double-layer clouds in China Xi'an was studied. The study on 11cases of seeder-feeder processes shows that the processes can be divided into three categories by defining the height difference (HD) between the seeding cloud base and the feeding cloud top, and the effective seeding depth (ESD). Through the analysis on the reflectivity factor and the radial velocity of cloud particles detected by MMCR and on the retrieved cloud dynamics parameters (vertical velocity of airflow and falling velocity of cloud particles), it is shown that the reflectivity factor in the cloud are significantly enhanced during the seeder-feeder period for the three types of processes. But there are different enhancements among the reflectivity factor profiles for the three seeder-feeder processes. The results also showed the limited depth as seeders entering the top of the feeding cloud. The lower and thinner the HD height was, the lower and thicker the ESD height was. On the contrary, the higher the HD height, the higher and thinner the ESD height.

Keywords: Macro parameters of cloud; Natural seeder-feeder process; Ka-band millimeter-wave cloud radar; Remote sensing and sensors

1. Introduction

Natural ice crystals in upper clouds can be a source of seeders for lower clouds (Korolev et al., 1999; Heymsfield et al., 2013; Myagkov et al., 2016; Cheng et al., 2020; Wang et al., 2023). This seeder-feeder process is able to lead the development of the lower clouds even to stimulate extreme precipitation (Choularton et al., 1986; Locatelliet al., 1983; Robichaud al., 1988; Fernández-González et al., 2015; Ramelli et al., 2021). The seeder-feeder process is a

https://doi.org/10.5194/egusphere-2023-2183
Preprint. Discussion started: 16 November 2023

phenomenon that ice crystals as seeders, either liquid, ice or mixed phase, from an upper cloud fall into a lower cloud or a lower-lying part of the same cloud (Hall et al., 1976; Korolev et al., 2003; Hong et al., 2005; Geerts et al., 2015; Lowenthal et al., 2018). When these seeders meet lower cloud droplets with ice phase or in supercool water state, the droplets will grow larger by riming or vapor deposition via the Wegener-Bergeron-Findeisen effect (Bergeron 1935; He et al., 2022). Therefore, it is important to understand the mechanism of the seeding-feeding process, which can be helpful to improve the representation of cloud processes in weather and climate models, and to weather forecasts of precipitation and ultimately to reduce uncertainty in climate simulations (Hong et al., 2005,2006 and 2012; Proske et al., 2021). The seeder-feeder mechanism has been studied by operations of the artificial precipitation enhancement, and it was found that the distinct changes in both cloud and precipitation properties based on observations from ground sites, aircraft, and satellite before and after the cloud seeding (French et al., 2018; Ramelli et al., 2021; Dong et al., 2021).

Historically, Braham (1967) noted the natural phenomenon of ice crystals from the upper cirrus clouds acting as seeders for ice formation in warmer clouds below. It was found that not only cirrus but also altocumulus and altostratus, which contain ice crystals, may act as the seeding clouds. In the 1980s in China, Hong et al., (2005 and 2006) established a cloud model that simulated the formation of stratiform clouds, which emphasized the seeder-feeder process. Subsequently, this cloud seeding process through sedimenting ice crystals has been observed in a multitude of remote sensing and aircraft campaigns. Seifert et al., (2014) and He et al., (2022) estimated the occurrence frequency of the natural cloud seeding through analyzing their lidar datasets. Furthermore, a regional occurrence frequency of seeder-feeder in the Arctic was estimated by Vassel et al. (2019). They pointed out that the seeder-feeder process happened usually within multi-layer clouds, which was observed by radiosonde and radar in Svalbard. By using the DARDAR satellite products and sublimation calculations, Proske et al., (2021) also studied the occurrence frequency of cloud seeding in Switzerland and found the high occurrence frequency of seeding situations with the survival of the ice crystals. The microphysical parameters of the seeder-feeder process appeared within mixed-phase clouds have been investigated by using the ground-based remote sensing instruments (Ramelli et al., 2021). However, there is still a lack of the specific characteristics to represent the seeder-feeder process including both the microphysics and thermodynamics.

Actually, the seeder-feeder process within clouds is not well documented in the literature (Hill et al., 2007; Purdy et al., 2005; He et al., 2022). The main reason is that the effects of the seeder-feeder process are not easy to be measured, because several cloud layers need to be able to monitor simultaneously with high vertical and temporal resolution. The active instrument of the Ka-band millimeter-wave cloud radar (MMCR), a useful tool for cloud observations, is capable of detecting multiple cloud layers directly, which allows measure the seeder-feeder process (Ramelli et al., 2021; Proske et al., 2021). The Doppler spectral data (*SP*) generated by MMCR can be used to retrieval the velocity of cloud particles and to obtain information of particle types (Luke et al., 2013; Shupe et al., 2008; Kollias et al., 2002 and 2011). However, such direct observations of ice crystal formation and evolution in the seeder-feeder process are limited (French et al., 2018).

In this study, the seeder-feeder processes happened between bilayer stratiform cloud in Xi'an were studied by using observation data from the MMCR together with microwave radiometer (MWR) and radiosonde measurements from January 2021 to December 2022. The parameters of microphysics, dynamics and thermodynamics during the seeder-feeder process were focused on analysis. In this paper, following the above review of study status on the seeder-feeder process, the used instruments and methods associated with datasets are introduced simply, then through a case analysis of seeder-feeder process measured by MMCR to expose the evolution mechanism of seeding cloud and feeding cloud. The main results and conclusions will be represented by statistics with two years data.

2. Instruments and methods

The instruments used in this study are MMCR, MWR, radiosonde and Raindrop Spectrometer (RDS). The MMCR is the Doppler vertical pointing cloud profile radar with solid-state transmitter. The main parameters of the MMCR are shown in Table 1. The MMCR can observe reflectivity factor (*Z*), radial velocity (V_r), *SP* and spectral width (σ). These parameters can be used to retrieve cloud dynamic parameters, such as cloud particle terminal velocity and vertical velocity of airflow inside the cloud (Liu et al., 2019; Yuan et al., 2022; Di et al., 2022). Because of the advantages of solid-state transmitter, the MMCR is small in size, long in life and good in reliability, so it provides reliable observational data for this study. Due to the MMCR has certain penetrating ability to cloud, it can detect the structure variation of multi-layer cloud system, so the phenomenon of seeder-feeder between multi-layer cloud system can be measured, which is an important reason for us to choose this instrument in this study.

The MWR includes 21 water vapor channels (distributed in K band, that is, 22–31 GHz), 14 air temperature channels (distributed in V band, that is, 51~59 GHz), and 1 infrared channel. The observations data of MWR can be used to retrieve the profiles of atmospheric temperature (/K) and humidity (/%), integrated water vapour content (Vint /mm) and integrated liquid water content (Lqint /mm). Below the height of 2 km, the root mean square error (RMSE) of temperature measurement is less than 1 K, the RMSE of temperature measurement is less than 1.8 K above 2 km height. The RMSE of relative humidity is less than 15 %, and the RMSE of integrated total water vapor is less than 4 mm. The relevant parameters of MWR are shown in Table 2.

https://doi.org/10.5194/egusphere-2023-2183
Preprint. Discussion started: 16 November 2023

Table 1 Major parameters of the MMCR

Order	Items	Technical specifications
1	Radar system	Coherent, pulsed Doppler; solid-state transmitter; and pulse compression
2	Radar frequency	35 GHz ± 200 MHz (Ka-band)
3	Antenna aperture	≥1.6 m
4	Horizontal and vertical beam width	0.4°and 0.4° beam width
5	Antenna gain	53 dB
6	Pulse repeat frequency	8000 Hz
7	Peak power	≥20 W
8	Detecting parameters Detection capability	*Z*, *Vr*, *σ*, and *SP* ≤ −35 dBz at 5 km
9	Range of detection	Height: 0.15 – 15 km Reflectivity: −45 – + 30 dBz Radial velocity: −15 – 15 ms^{-1} Spectrum width: 0–15 ms^{-1}
10	Spatial and temporal resolutions	Temporal resolution: 5 s Height resolution: 30 m
11	Pulse width	1 µs; 5 µs; and 20 µs

Table 2 Major technical parameters of MWR

Order	Items	Technical specifications
1	Range of detection	0 – 10 km
2	Height resolution	≤ 25 m (0~ – 500 m) ≤ 50 m (500 – 2000 m) ≤ 250 m (2 – 10 km)
3	Layering	≥83 layers
4	Channel frequency	K-band: 22 – 31 GHz V-band: 51 – 59 GHz
5	Number of channels	number of water vapor channel: 12 number of temperature channel: 14 number of infrared channel: 1
6	Absolute brightness temperature accuracy	≤1.0 K
7	Temperature profile error	≤ 1.8 K， Range >2 km ≤ 1.0 K， Range ≤2 km
8	Humidity profile error	≤15%
9	Integral total water vapor error	≤4 mm

The above instruments were placed at the Jinghe National Meteorological Station (108°58’E, 34°26’N, as shown in Fig. 1) in Xi'an, Shaanxi Province, China, which is located near the north bank of the Wei River in Guanzhong Basin (between 107°40’–109°49’E, 33°42’–34°45’N, about 400 meters above sea level) in the middle of the Yellow River Basin. The Qinling Mountains on the south side of the Wei River often block the cold air southward in winter and spring, and produce stable stratiform clouds in the Guanzhong Plain, which provides a natural experimental site to study the phenomenon and mechanism of seeder-feeder of bilayer stratiform clouds. The distance between MMCR and MWR is less than 5m, and the distance between other instruments is less than 50 m. The Jinghe National Meteorological Station is also the national Meteorological sounding Station. Sounding balloons are released every day at 07:15 and 19:15 BJT (Beijing Time) to detect atmospheric temperature, humidity, wind speed and direction from the ground to an altitude of 30 km above the station (Görsdorf et al., 2015; Vassel et

https://doi.org/10.5194/egusphere-2023-2183
Preprint. Discussion started: 16 November 2023

al. 2019; Yuan et al. 2022). The collaborative detection of the above instruments provides effective data support for capturing the seeder-feeder process in clouds and its mechanism in this study.

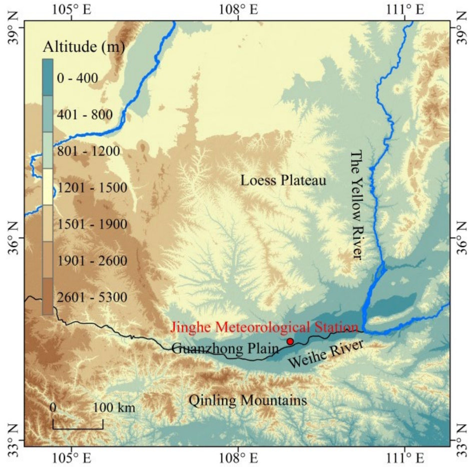

Figure 1 Geographical coverage of Shaanxi Province (105°29'-111°15'E, 31°42'-39°35'N). The red dot indicates the location of the Jinghe National Meteorological Station in Xi'an (107°40'-109°49'E, 33°42'-34°45'N).

As the MMCR adopts vertical upward mode observation, its echo signal will not be affected by ground clutter, which reduces the trouble of eliminating terrain clutter in observation data quality control. However, due to the influence of air haze and insects in lower atmosphere, there will be non-cloud signals in the bottom echo signal of the MMCR. Therefore, the multi-dimensional threshold information (based on non-cloud signal reflectivity factor, radial velocity, spectrum width and signal-to-noise ratio) was used for quality control of echo signal, and eliminate these non-cloud signals to obtain accurate cloud information (Yuan et al., 2022). The *SP* measured by MMCR includes the information of the cloud particle falling velocity and the vertical velocity of airflow. The *SP* is also affected by radar beam width, ambient wind shear and atmospheric turbulence. Therefore, radiosonde data combined with the MMCR hardware parameters were used to correct the broadening of *SP*, in order to improve the accuracy of the retrieved vertical velocity of airflow and the particles falling velocity in clouds (Doviak and Zrnic, 1993; Shupe et al., 2008; Kollias et al., 2001 and 2002; Shupe et al., 2008 and 2004).

To calculate the vertical velocity of the airflow in the cloud more accurately, the cloud phase state was judged. Because the descending the cloud particles velocity in different phase states is different, the influence on the vertical velocity of the airflow in the cloud is different. Cloud particle phase identification adopts cluster analysis method (Yuan et al., 2022). The specific process takes cloud reflectivity factor, particle radial velocity and spectrum width measured by the MMCR, and atmospheric temperature measured by MWR as input parameters for cloud phase identification. Through unsupervised learning, cloud particles of different phase states in the cloud were identified, such as warm clouds, mixed phase (ice dominated phase and water dominated phase), ice, supercooled water, drizzle, rain and graupel particles. In the identified ice particle region and mixed phase region, the small particle tracer method was used to obtain the vertical velocity of the airflow (Shupe et al., 2008).

In the identified l supercooled water region, the peak position of the liquid cloud particle is used to obtain the vertical velocity of airflow (Guo et al., 2019). When there was a drizzle, the *SP* of MMCR usually shows a bimodal distribution, and the vertical velocity of the airflow in the cloud can be obtained by the bimodal position of the liquid cloud particles (Wei et al., 2019; Luke et al., 2010 and 2013). The velocity of falling cloud particles and the vertical velocity of airflow are important parameters in analyzing the seeder-feeder process. Based on the observation data of MMCR from 2021 to 2022 (a total of 10363 hours), the seeder-feeder process of bilayer cloud system (ice phase in upper cloud and mixed phase cloud in lower cloud) will be analyzed below.

3. Parameter Definition and Case Analysis

To conveniently and clearly analyze the seeder-feeder process of bilayer clouds in Xi 'an, and find how the upper seeding clouds to seed the lower feeding clouds in this study. We have chosen observational data of MMCR and MWR in winter and spring, as most of the clouds in this season are stable stratiform clouds. The first step is to define the relevant parameters to describe the characteristics of the bilayer clouds, such as the top height of seeding cloud (THSC) and the base height of seeding cloud (BHSC), the top height of feeding cloud (THFC). The height difference (DH) between the height of the seeding cloud bottom and the height of feeding cloud top is also defined. The DH can display directly one of the geometric features of the bilayer clouds. A period of stable time before the seeding cloud began to seed was denoted as t1, the moment when the seeding cloud began to seed was marked as T0, the length of time period of the seeding was denoted as t2, and the period after the end of the seeding but the lower part of the feeding cloud still showed development changes in reflectivity factor was labeled as t3 (which is called the duration of the seeding effect). Fig. 2 shows the cloud reflectivity factor and radial velocity detected by MMCR from 23:00 BJT on 05 February, 2022 to 04:00 BJT on 05 February, 2022. The reflectivity factor (Fig. 2a) clearly shows the seeder-feeder process. The period from 00:40 to 02:20 BJT, cloud particles of the bottom of the upper cloud fall into the top of the lower cloud. This is confirmed by the cloud particle radial velocity (Fig. 2b), which shows that the cloud particles during the period are all sinking, and the sinking velocity is about 1ms^{-1}. The above defined parameters have been marked in Fig. 2a. It also shown that the bilayer cloud is stable during this period, with THSC stable at 8 km, BHSC at 5.5 km, THFC at 4.2 km, DH at 0.85 km, seeding time t2 at 98.2min, and feeding cloud development duration at more than 2hr 30min. Before seeder-feeder process of the bilayer clouds, only 40 minutes (t1) is considered as the earlier state of beclouds, as detailed in Table 3.

https://doi.org/10.5194/egusphere-2023-2183
Preprint. Discussion started: 16 November 2023

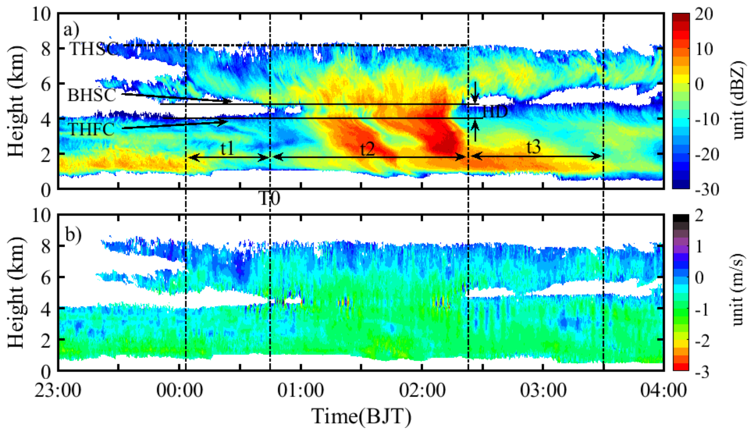

Figure 2 The variations with time for both profiles of cloud reflectivity factor (a) and cloud particle radial velocity (b) detected by MMCR from 23:00 BJT on 05 February, 2022 to 04:00 BJT on 06 February, 2022 (positive value in color bar represents ascending motion and negative value represents sinking motion). In the figure, THSC and BHSC are the cloud top height and cloud base height of the seeding cloud, THFC is the cloud top height of the feeding cloud, and HD is the height difference between the bottom height of seeding cloud and the top height of feeding cloud. T0 is the moment when the seeding cloud began to seed, t1 is the stable time period before the seeding cloud begins to seed, t2 is the length of time from the beginning to the end of the seeding, and t3 is the period after the end of the seeding but the reflectivity factor in the feeding cloud still development.

Table 3 Values of the defined parameters for the seeder-feeder process observed by MMCR from 23:00 BJT on 05 February, 2022 to 04:00 BJT on 06 February, 2022.

Parameters	THSC /(km)	BHSC /(km)	THFC /(km)	HD /(km)	t1 /(min)	t2 /(min)	t3 /(min)
Values	8.2	5.1	4.3	0.85	40.2	98.2	44

In order to reveal the variation characteristics of the cloud system during this seeder-feeder process, the spectrum width of cloud particles, vertical velocity of the airflow, and the final falling velocity of cloud particles were firstly calculated from the signals of the *SP* detected by MMCR (as shown in Fig. 3, the positive value of the velocity is specified as the ascending motion and the negative value is the descending motion). Fig. 3a shows that the spectrum width is small, indicating that the cloud particle radial velocity detected by MMCR is relatively stable, which also indicates that the airflow inside bilayer clouds is stable. The maximum velocity spectrum width is about 0.6 ms^{-1}, which is mainly located at the top of the seeding and feeding clouds (especially at the beginning of the feeding cloud), and the lower part between the seeding and the feeding cloud during the seeding period (that is, the top of the feeding cloud). In addition, the feeding cloud showed changes in the t3 period after seeding, that is, the feeding cloud top height rose slightly (Fig. 2a), and the spectrum width increased at the cloud top zone, which says that the radial velocity at this zone changed greatly during the t3 period. This is probably because of latent heating release by the phase transition in the seeding cloud during seeder-feeder process, which will be feedback the dynamic process, then increases the vertical velocity of the air low inside the cloud. This position in Fig. 3b indeed indicates that the vertical velocity of the airflow is relatively large (0.5–2 ms^{-1}). Fig. 3b shows that weak upward movement (0.5–2 ms^{-1}) prevails in the seeding clouds and the feeding clouds, which is consistent with the dynamic

https://doi.org/10.5194/egusphere-2023-2183
Preprint. Discussion started: 16 November 2023

structure characteristics of stable stratiform clouds (Hou et al., 2010; Wang et al., 2022) in winter and spring in Xi'an region. The maximum vertical velocity of airflow was located at the junction of upper and lower clouds, the top and bottom of feeding clouds and the top of seeding clouds in t3 period. During the seeding period, the middle and lower zones of the feeding cloud also has a large airflow upward movement (up to 1.5 ms^{-1}). The airflow sinking movement is rarely seen in the bilayer cloud in the vertical. But in some altitudes, there are the airflow sinking movements, which can be explained the needs of airflow sinking movement short-term to achieve mass balance. Fig. 3c clearly shows the cloud particles in the seeding cloud sink to the feeding cloud, and the sinking velocity of the cloud particles is in the range of –1~ –4 ms^{-1} during seeding process. During this seeding process, 00:45–01:50 BJT and 02:00–02:20 BJT are two significant seeding periods, and the maximum sinking velocity of cloud particles is about –4 ms^{-1} in last period indicating seeding intensity. According to Table 2, the height difference (HD) between seeding and feeding cloud is 0.85 km. If the sinking speed of cloud particles is at –2 ms^{-1}, it takes about 7 minutes for cloud particles to fall from the seeding cloud bottom to the feeding cloud top. In addition, Fig. 2 and Fig.3 show that seeding end at 02:20 BJT, but Fig. 3c still shows that after this time, cloud particles still sink (at 02:45 BJT, sinking velocity –0.5 ms^{-1}) on the feeding cloud top. It is likely that MMCR is limited in its sensitivity to detect smaller particles and cannot clearly show the reflectively factor of small particles. The above results indicate that the sinking motion region (time period) of the cloud particle's final falling velocity can be used to identify the seeding cloud effectively. Anyway, the above gives an important conclusion, i.e. after seeding, the feeding cloud top rose slightly, which may be the result of latent heating release. The sinking motion zone of particle final velocity can directly characterize the seeding process.

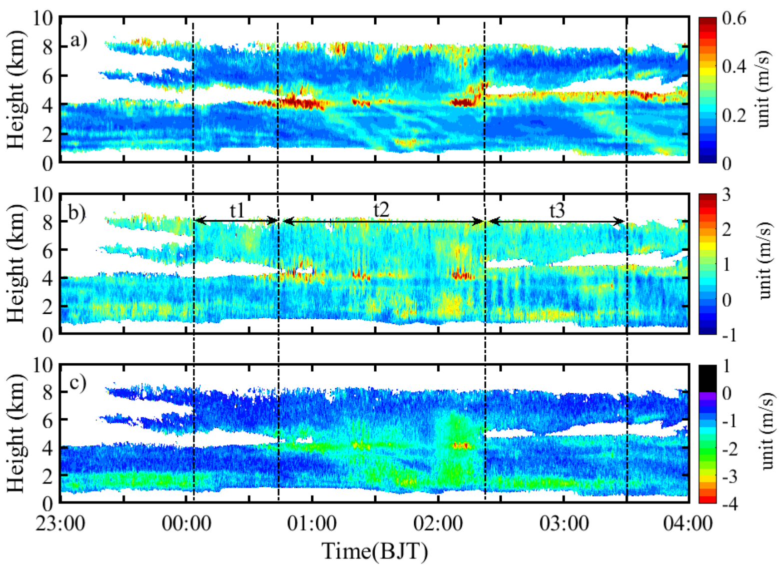

Figure 3 The spectrum width of cloud particles (a), vertical velocity of the airflow (b), and the final falling velocity of cloud particles (c) based on the retrieval from MMCR (positive value in the color bar represents ascending motion and negative value represents sinking motion) .

https://doi.org/10.5194/egusphere-2023-2183
Preprint. Discussion started: 16 November 2023

By using the data of MMCR and MWR observations, the phase state and water vapor structure of the cloud, the total amount of liquid water and water vapor in the column can be retrieved. Fig. 4a shows that seeding clouds consist of ice and snow, and seeding is caused by sinking ice particles. Before seeding, the particles in the feeding cloud were basically in mixed phase, and there was a thin layer of supercooled water in the middle and upper part of the cloud, and snow particles appeared at the bottom of the cloud for a short time after 00:10 BJT. During being seeded, ice particles were the main component in the cloud. After being seeded, the ice particles in the lower part of the feeding cloud lasted for a long time (maintaining the whole t3 period), while the supercooled water layer at the top was obvious. The temperature of the supercooled water layer is close to –20°C, while that of the seeding cloud top is close to –40°C. The instantaneous water vapor flux structure (Fig. 4b) indicates that the seeding cloud is smaller than the feeding cloud, and the bottom layer of the feeding cloud has an instantaneous water vapor flux greater than 20 $gm^{-2}s^{-1}$, indicating that the lower layer of the atmosphere has high humidity during the seeing-feeding process in bilayer stratiform cloud. The temporal variation of column water vapor and column liquid water given by MWR (Fig. 4c) showed that both rapidly increased from t1 before seeding to the beginning of seeding, and rapidly decreased after seeding. Before the second intense seeding, column water vapor and column liquid water increased rapidly, and then decreased with the end of seeding. This process can be understood as that when the ice phase particles of the seeding cloud enter the supercooled water of the feeding cloud top, the Bergeron effect is triggered, and the liquid particles are rapidly transformed into ice phase particles, which leads to the reduction of liquid water content in the column. Therefore, the Bergeron effect is the main reason for the reduction of liquid water content in the column. The above results illustrate that the seeders of seeding cloud causes the change of cloud phase state in the feeding cloud, thus reducing the water vapor and liquid water in the column. The rapid increase of water vapor and liquid water in the column before seeding may be related to the change of atmospheric environment at that time, which still needs to be studied in detail.

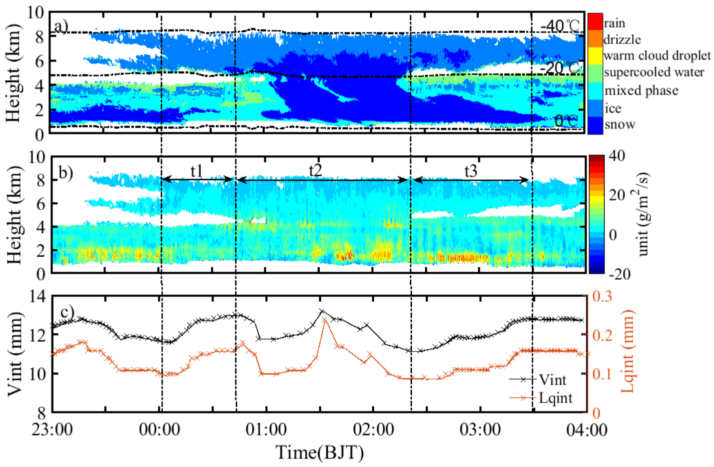

Figure 4 The variations of cloud phase (a), water vapor flux (b), integrated water vapour content (Vint: black line) and integrated liquid water content (Lqint: Orange line) (c) with time observed and retrieved by MMCR and MWR.

According to the radar formula, the echo signal intensity is proportional to the sixth square of the cloud particle diameter. The cloud particle with larger diameter has a larger falling speed under the action of gravity. In order to reveal the relationship between cloud particle microphysical parameters and echo signals in the process of seeder and feeder, such as calculating the reflectivity factor profile and cloud particle parameter profile, the statistical classification method of equal samples is adopted, that is, all samples are arranged according to the order of small to large, and then arithmetically average based on the proportion. For example, the first 33%, middle 33% and last 33% of the sample are arithmetically averaged to obtain the mean reflecting the weak, moderate and strong values respectively. This has the advantage of avoiding the defect of large and small arithmetic averages cancelling each other out. Following to this principle, the reflectivity factors of t1, t2 and t3 are arranged in ascending order, and the corresponding microphysical parameters of cloud particles are also sorted with the order of reflectivity factors, and then the arithmetic average is performed according to the first 33%, middle 33% and last 33% of the sample. The average profile representing weak echo, moderate echo and strong echo (as shown in Figs 5a1, a2, a3) is obtained, and the corresponding average profile of cloud particle parameter profile for the three intensity echoes is also gained, the same to the corresponding average profile of cloud particle radial velocity (Figs 5b1, b2, b3), average profile of velocity spectrum width (Figs 5c1, c2, c3), average profile of final falling velocity (Figs 5d1, d2,d3) and average profile of vertical velocity of the airflow (Figs 5e1, e2, e3).

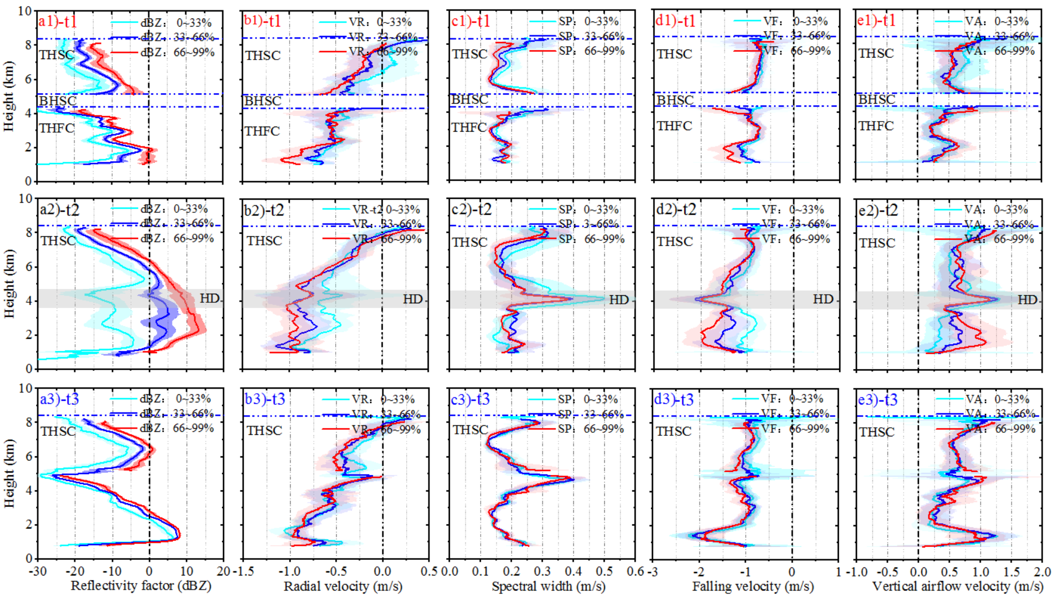

Figure 5 The mean profiles of reflectivity factor (a1, a2, a3), radial velocity (b1, b2, b3), spectrum width (c1, c2, c3), final falling velocity (d1, d2, d3) and vertical velocity of the airflow (e1, e2, e3) during t1 (up), t2 (middle) and t3 (bottom) periods, respectively. In the figure, the cyan line, blue line and red line represent the average of the first 33%, the middle 33% and the last 33% of the sample respectively; the solid line represents the mean, and the shaded area of the corresponding color is the variance.

https://doi.org/10.5194/egusphere-2023-2183
Preprint. Discussion started: 16 November 2023

The up panel of Fig. 5 shows that there are obvious differences (a1) between the weak, moderate and strong reflectivity factor profiles of seeding clouds and feeding clouds before seeding (t1 period), but in general, the average profiles of the three kinds of echo intensity show that reflectivity factor increases with the decrease of height, and the values of the profiles are relatively small (all less than 0 dBZ) and the variance is also small. However, the profiles of cloud particle radial velocity (b1), spectral width (c1), final falling velocity (d1) and vertical velocity of the airflow (e1) corresponding to the average profiles of the three intensity reflectivity factors basically coincide, and do not show significant changes in these parameters caused by differences in reflectivity factors. This indicates that the cloud particle states (radial velocity, spectrum width, final falling velocity and vertical velocity of airflow) of seeding and feeding clouds in t1 period are uniformly distributed at different intensity echoes, that is, the upper and lower cloud systems are stable before seeding, and the size of cloud particles is mainly small.

The middle panel Fig. 5 represents the average profile of each parameter during the seeding period (t2). Fig. 5 a2 shows that the difference between the average profiles of the reflectivity factors for the three kinds of echo intensity is greater than that before seeding. In particular, the profile of the moderate and strong reflectivity factors in the figure increases significantly, reaching a maximum of 15 dBZ, which hints that the size distribution of cloud particles in the bilayer cloud varies significantly during seeding. Compared with before seeding, the reflectivity factor of the lower part of the seeding cloud (5.4 km ~ 6.2 km) increased significantly, and the radial velocity of cloud particles (Fig. 5 b2), the final falling velocity of cloud particles (Fig. 5 d2) and the vertical velocity of airflow (Fig. 5 e2) all increased correspondingly. It was these changes of cloud particles under the seeding cloud that produced the seeding effect. Relatively, the spectral width of cloud particle velocity (Fig. 5 c2) changes little with height, which alludes to the relatively uniform of the particle falling velocity. For the strong reflectivity factor profile, from the top of the seeding cloud to the lower part of the feeding cloud at a height of 2 km, reflectivity factor increases rapidly with the decrease of the height, and the corresponding radial velocity and final velocity of the cloud particles increase (i.e. the descending velocity increases), and the vertical velocity of the airflow also increases, indicating that the large particles in the seeding cloud have a great effect on the feeding cloud. For the weak reflectivity factor profile of bilayer cloud, the average reflectivity factor changes little compared with that before seeding, indicating that the seeding effect of small cloud droplets corresponding to such weak echoes is small. Fig. 5 also shows that during the seeding period, the reflectivity factor of the middle and upper part of the feeding cloud increases significantly after the seeders is injected into the feeding cloud, especially in the case of strong and moderate intensity, indicating that the middle and upper part of the feeding cloud particles become significantly larger, which clearly expresses the seeding effect.

With the end of seeding (bottom panel in Fig. 5), the reflectivity factor of the upper and middle part of the seeding cloud decreased significantly. The reflectivity factor of the lower part of the feeding cloud increased, which reveals that the seeding effect developed to the lower part of the feeding cloud. In general, the distribution of strong, moderate and weak reflectivity factor profiles in feeding clouds was concentrated after seeding, informing that cloud particle size became more uniform, which was obviously different from that before and during seeding. Therefore, the profiles of cloud particle radial velocity, velocity spectral width, final falling velocity and vertical velocity of the airflow corresponding to the strong, moderate and weak reflectivity factors basically coincide. The above results show that after the seeding, the cloud particle size distribution and particle velocity of the bilayer cloud reach a relatively balanced and stable state through complex thermodynamic and dynamic interactions. However, the reflectivity factor of the feeding cloud reaches the maximum in the lower layer (1 km~2 km), and the corresponding radial velocity and final falling velocity of cloud particles also reach the maximum, indicating that seeding effect continues at the bottom of the feeding cloud although seeding has ended at the top of the feeding cloud. The key takeaway from Fig. 5 is that the reflectivity factor (related to cloud particle scale) and the descending velocity of cloud particles increased within a certain depth of the feeding cloud during the seeding period. After the end of seeding, there was a seeding continuation period in the middle and lower part of the feeding cloud.

In order to understand the effect of seeding cloud on feeding cloud, the correlation coefficient between cloud particle falling velocity and reflectivity factor is calculated statistically. Firstly, the correlation coefficient between the final falling velocity of cloud particles at each elevation of the bilayer cloud during the seeding period (t2) and the reflectivity factor of the corresponding elevation layer (called the autocorrelation coefficient, because the final falling velocity of cloud particles has a certain relationship with the size of cloud particles, while the reflectivity factor is proportional to the 6th power of the particle diameter) was calculated. Therefore, the cloud particle falling velocity is not completely independent of the reflectivity factor. The obtained autocorrelation coefficient profile is shown in Figure 6a, which indicates that as the height decreases from the middle of the seeding cloud (6 km) to the middle and lower part of the feeding cloud (2.5 km), the autocorrelation coefficient increases from 0 to 0.8, that is, the positive correlation between the cloud particle descent speed and the reflectivity factor increases continuously. The reflectivity factor of the corresponding height also increases with the decrease of altitude (from –5 dBZ to 5 dBZ), illustrating the reflectivity factor and final falling velocity of cloud particles increase with the decrease of height, which may be inferred that the size of cloud particles also increases with the decrease of height. It can be seen that during the seeding period (t2), the reflectivity factor of the middle and upper part of the feeding cloud will be large and the particle falling velocity will increase. Therefore, the Effective Seeding Depth (ESD) is defined as the height difference between the top height of the feeding cloud and from the height down to the height of the maximum correlation coefficient, which represents the influence of seeders on the seeding cloud. In this case, the ESD is about 1.6 km. In the ESD region, the echo intensity increases with the decrease of the height, so the cloud particle size also increases rapidly with the decrease of the height, as the result the middle and lower part of ESD is

https://doi.org/10.5194/egusphere-2023-2183
Preprint. Discussion started: 16 November 2023

the area where the sowing effect is most intense. In the upper part of ESD (i.e. the top of the feeding cloud), the reflectivity factor is slightly smaller (less than 3 dBZ) and the correlation coefficient is also smaller (less than 0.2), indicating that the upper cloud particle size of the feeding cloud is small, and the correlation between the final falling velocity of the cloud particle and the reflectivity factor is poor, because the seeders has just entered the top of the feeding cloud and the seeding effect has just begun.

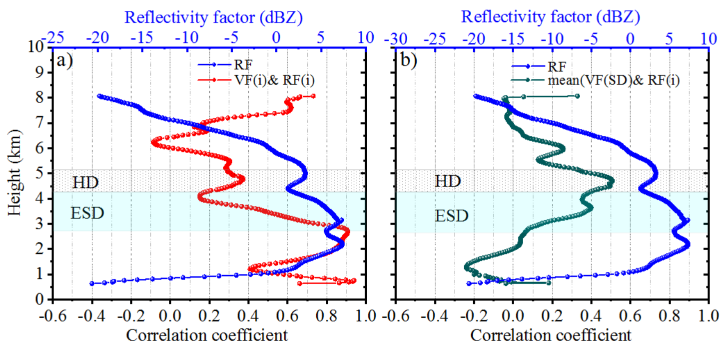

Figure 6. The autocorrelation coefficient profile (a) between cloud particle descent velocity and reflectivity factor at each layer from top to bottom in the bilayer cloud in t2 period, and the correlation coefficient profile (b) between the average descent velocity of cloud particle in the HD region and reflectivity factor at different height layers in t2 period.

If the region between the upper and lower clouds, i.e. HD region, is regarded as a whole layer, the correlation coefficient between the average final falling velocity of cloud particles in this layer and the reflectivity factors of cloud layers during the seeding period (t2 period) (called non-autocorrelation coefficient, because the final velocity of cloud particles and the reflectivity factors in the non-HD region are relatively independent at this time) is calculated, and the non-autocorrelation coefficient profile in Fig. 6b is obtained. It shows that above the height of the HD region, the positive correlation between the average final velocity of cloud particles and the reflectivity factor of each layer of the seeding cloud increases as the height decreases, indicating that the velocity of cloud particles in the HD region is mainly affected by the reflectivity factor of the lower layer of the seeding cloud. The larger the reflectivity factor of the lower layer of the seeding cloud is, the larger the velocity of cloud particles in the HD region, which conforms to the physical principle. As the height decreases to the bottom of the feeding cloud, the non-autocorrelation coefficient decreases from 0.4 to –0.2, indicating that the average final velocity of cloud particles in the HD region is only positively correlated with the reflectivity factor near the top of the feeding cloud, that is, cloud particles in the HD region only affect the clouds near the top of the feeding cloud, but have little effect on the lower part of the feeding cloud. This shows that the reflectivity factor in the middle and lower part of the feeding cloud has little correlation with the final velocity of cloud particles in the HD region. In generally, the effect of seeding cloud on feeding cloud is mainly manifested in the middle and upper part of feeding cloud, that is, the seeding effect activing in the effective seeding depth. During the seeding period, the cloud particle size is small (low reflectivity factor) from the top of feeding cloud upward to the 1km height. From top to bottom in the ESD,

https://doi.org/10.5194/egusphere-2023-2183
Preprint. Discussion started: 16 November 2023

the size of cloud particles increased (the reflectivity factor increased), indicating that seeding mainly occurred in this depth. After the end of seeding, the continuous influence of the seeding process in the feeding cloud can be understood as the delay of seeding benefits, and also can be understood as the seeding process inside the feeding cloud, that is, the seeding of the middle part of the feeding cloud to its lower part.

4. Statistical characteristics

To reveal the characteristics of the seeder-feeder process of bilayer cloud over the Shanxi-Guanzhong Plain, the observation results by MMCR from winter to the next spring from 2021 to 2022 were analyzed, because a large range of compact and stable stratiform clouds often appear in the region during this season. During the observation period, MMCR observed 11 cases of seeder-feeder process of stratiform clouds. Table 4 lists the specific time of seeder-feeder process, cloud top and cloud base height of the seeding cloud, cloud top height of the feeding cloud, height difference between upper and lower clouds, seeding start time, seeding duration and end time, cloud base phase of feeding cloud. According to the precipitation records observed by the surface rain gauge, Table 4 shows that there were 6 cases with precipitation occurrences (one with snowfall) after the seeder-feeder process occurred. In 4 cases, the height of the cloud base of feeding clouds dropped to about 560m, and the falling velocity of the cloud particles at the bottom of the cloud was measured to be $-2 \sim -3 ms^{-1}$, these cloud particles were liquid, so it can be seen that there were rain flags (drizzle that did not fall to the ground) at the bottom of the feeding clouds. In the process of 31 March, 2022, the echo intensity of the middle and lower part of the feeding cloud increased after seeding, and the cloud particles mainly moved down. However, due to the high height of the cloud base (about 3.9 km), the retrieved phase showed mixed phase, and no precipitation was observed by the ground rain gauge.

Table 4 Lists of the characteristic parameters of the seeder-feeder process for 11 cases of bilayer stratiform cloud from 2021 to 2022.

Case	Time	THSC /(km)	BHSC /(km)	THFC /(km)	HD /(km)	t1 /(min)	t2 /(min)	t3 /(min)	Phase in feeding cloud	Precipitation state
1	2021-11-29	10.23	6.00	5.20	0.80	101.5	91.3	114.9	rain	Yes
2	2022-02-06	8.20	5.10	4.30	0.80	40.2	98.2	44	ice	No
3	2022-02-06	8.43	5.61	4.86	0.75	49.1	113.9	33.6	snow	Yes
4	2022-04-30	9.21	5.80	4.84	0.96	73.6	65.1	34.1	rain flag	No
5	2022-11-16	8.79	5.71	4.77	0.94	23.7	36.3	9.0	rain flag	No
6	2021-01-23	9.45	6.12	4.50	1.62	80.3	59.6	29.5	rain flag	No
7	2021-03-10	11.04	7.21	6.06	1.15	67.9	138.0	45.3	rain	Yes
8	2022-03-31	10.02	7.74	6.25	1.49	30.3	30.9	23.3	mixed phase	No
9	2022-06-04	10.23	6.99	5.43	1.56	15. 7	41.7	13.4	rain	Yes
10	2022-04-24	10.62	9.26	8.15	1.11	30.0	103.1	41.8	rain	Yes
11	2022-11-08	10.65	8.04	5.82	2.22	35.8	47.0	17.5	rain	Yes

https://doi.org/10.5194/egusphere-2023-2183
Preprint. Discussion started: 16 November 2023

Table 5 Statistical results of characteristic parameters of three types of seeder-feeder processes.

Type	Samples	Variable	THSC /(km)	BHSC /(km)	THFC /(km)	HD /(km)	t1 /(min)	t2 /(min)	t3 /(min)
I	5	Mean	8.97	5.64	4.79	0.85	58	81	47
		RMSE	0.51	0.09	0.08	0.01	741	747	1282
II	4	Mean	10.18	7.02	5.56	1.46	60	68	28
		RMSE	0.33	0.34	0.47	0.03	452	1756	134
III	2	Mean	10.64	8.65	6.99	1.67	33	75	30
		RMSE	0.00025	0.37	1.36	0.31	8	787	148

Based on the characteristic parameters of seeding cloud and feeding cloud listed in Table 4, the seeding process can be generally divided into three categories according to the height of seeding cloud base and the height difference (HD) between upper and lower clouds. The seeding process of type I has low seeding height ((BHSC<6 km) and small HD (HD⩽1km), the type II has higher seeding height (6km⩽BHSC＜8km) and larger HD (HD⩾1km), and the type III also has higher seeding height (BHSC⩾8 km,) and larger HD (HD⩾1km). The Table 5 shows the characteristic parameter distributions of these three types of seeder-feeder processes. The average thickness of HD in the type I is 0.85km, the average length of seeding time t2 is 81min, and the average duration of seeding effect time t3 is 47min (the longest among the three types of seeder-feeder processes). The average HD thickness of class III is the deepest (1.67 km), and the duration of seeding time t2 and seeding effect duration t3 are longer than those of Class II.

In order to expose the internal mechanism of the seeder-feeder process, the contour frequency by altitude diagram (CFAD) with height for the reflectivity factor, radial velocity, spectral width, final particle falling velocity and vertical velocity of air flow in these three types of seeder-feeder parameters were calculated and plotted. Figs 7a1, 7b1 and 7c1 show the differences in the distribution of reflectivity factor with height in the three types before seeding. The differences of the HD depth and its height before seeding were clearly shown, and the reflectivity factor of feeding cloud before seeding was small. Figs 7a2, 7b2 and 7c2 clearly show that the reflectivity factor of both seeded and seeded clouds increase during the seeding period, especially the height of the cloud base of the feeding clouds decreases significantly, indicating that the development of seeded clouds caused by seeding is likely to cause precipitation. After seeding, the reflectivity factor of seeding clouds weakened and their thickness thinned (even disappeared in the type III), but the lower part of feeding clouds continued to develop (Figs 7a3, 7b3, 7c3), especially in the type I. The above shows that when the HD is small and its height is low (type I), the seeding cloud has the greatest influence on the seeded cloud, because in this case, the distance between the seeding cloud and the feeding cloud is short, and the seeders are easy to affect the seeded cloud.

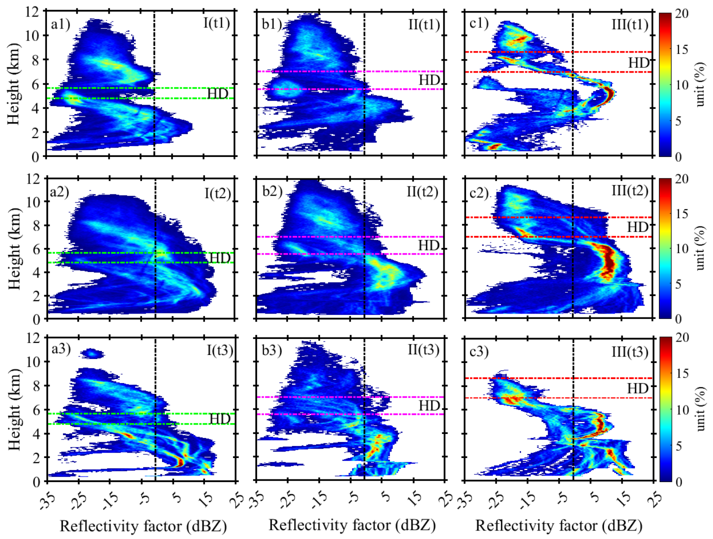

Figure 7 The CFAD of reflectivity factor in three types of seeder-feeder process before (t1), during (t2) and after (t3) seeding. The f type I (5 cases) on the left column, the type II (4 cases) in the middle column, and the type III (2 cases) in the right column. Note: the HD of type I is thin and low in height, the HD of type II is thick and slightly higher in height, and the HD of type III is thick and the highest in height, the same below.

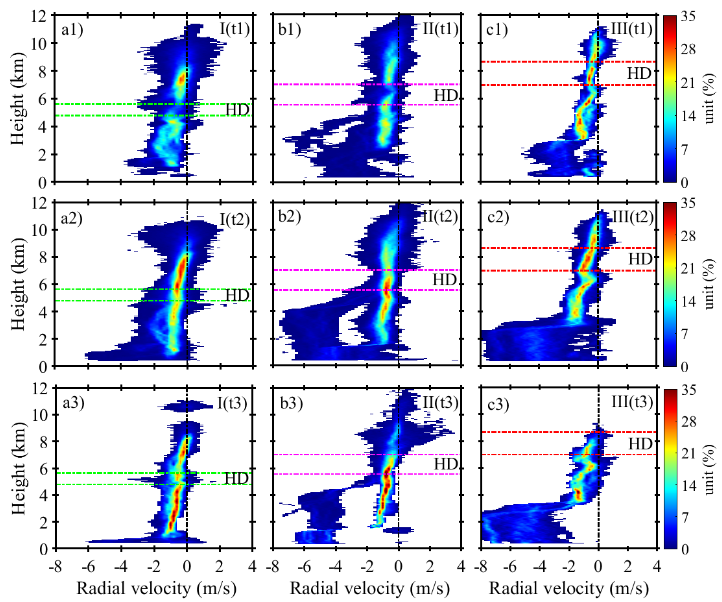

Figure 8 The CFAD of radial velocity in three types of seeder-feeder process before (t1), during (t2) and after (t3) seeding.

The cloud particle radial velocity detected by MMCR is the actual motion velocity of cloud particles in the cloud, which can be understood as the synthesis rate of the air flow velocity and the falling velocity of cloud particles under the action of gravity. The probability density distribution with height of the cloud particle radial velocity in

https://doi.org/10.5194/egusphere-2023-2183
Preprint. Discussion started: 16 November 2023

three types is plotted in Fig. 8, which shows a weak rising movement in the upper part of the seeding cloud before seeding in three types, while a weak sinking movement appears in the lower part. In the feeding cloud, a weak subsidence exists consistently with slightly larger near the ground. In general, the radial velocity of most cloud particles in seeding cloud and feeding cloud keeps sinking motion, and the sinking motion increases with decreasing height. The radial velocity of cloud particles in seeding cloud and feeding cloud remained the same as before seeding. However, after seeding, the negative radial velocity of cloud particles decreased (subsidence motion increased) in the first type both seeding clouds and feeding clouds, the same to the second and third types. In the meantime, seeding clouds disappeared in the third type (consistent with Fig. 7c3). The most important feature is that the radial velocity of cloud particles increases with the decrease of height from before seeding to seeding process and after seeding for the three types of seeing-seeding process. After seeding, the negative radial velocity of cloud particles in the lower part of the feeding cloud decreased significantly.

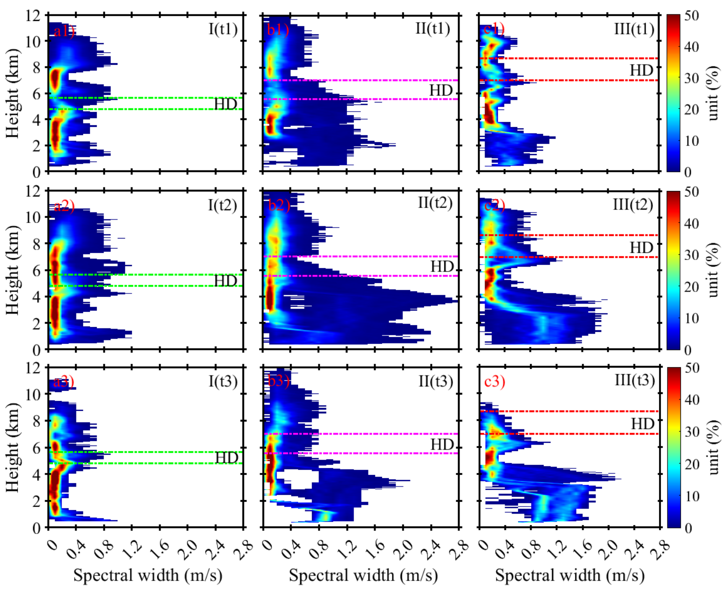

Figure 9 The CFAD of spectral width in three types of seeder-feeder process before (t1), during (t2) and after (t3) seeding.

The velocity spectral width of cloud particle detected by MMCR reflects the distribution range of cloud particle velocity. A larger value indicates a large change in cloud particle velocity, while a smaller value indicates uniform cloud particle velocity. Fig. 9 shows the distribution of the probability density with height for the velocity spectral width in the three types of seeding and feeding clouds. The figure shows that the velocity spectral width of most clouds in the seeding and feeding clouds is less than 0.4 ms^{-1}, and the distribution of particle velocity spectral width in the type I is the narrowest (most of them are less than 0.2 ms^{-1}). Moreover, the velocity spectral width did not

https://doi.org/10.5194/egusphere-2023-2183
Preprint. Discussion started: 16 November 2023

change significantly before and during seeding (Figs 9a1 and a2). But it became significantly narrower after seeding (Fig. 9a3), which indicates a relatively uniform of the velocity of cloud particles. That was consistent with the concentrated distribution of probability density for the radial velocity of cloud particles with height as shown in Fig. 8 a3. The velocity spectral width of the second and third types is wider than that of the type I. The maximum of the velocity spectral width reaches more than 1.6 ms^{-1}, and the velocity spectral width in feeding clouds is wider than that in seeding clouds, i.e. the velocity of cloud particles in feeding clouds is greatly different. In the process of seeding, the velocity spectral width of cloud particles for the type II and III became significantly wider (Figs. 9b2 and c2), which is an evidence of the seeding effect resulting in a wide velocity distribution of cloud particles within the feeding cloud. After seeding, the velocity spectral width in feeding cloud of the both types still remained relatively wide (Figs. 9b3 and c3). In the HD area, the velocity spectrum width is wider in the type II and III than in the type I during seeding, which may portend a wider distribution of the cloud particle size in the second and the type III. While in the top of the feeding cloud, there is a small velocity spectrum width for the three types, which hints the relatively uniform of cloud particle velocity and the narrow distribution of cloud particle sizes.

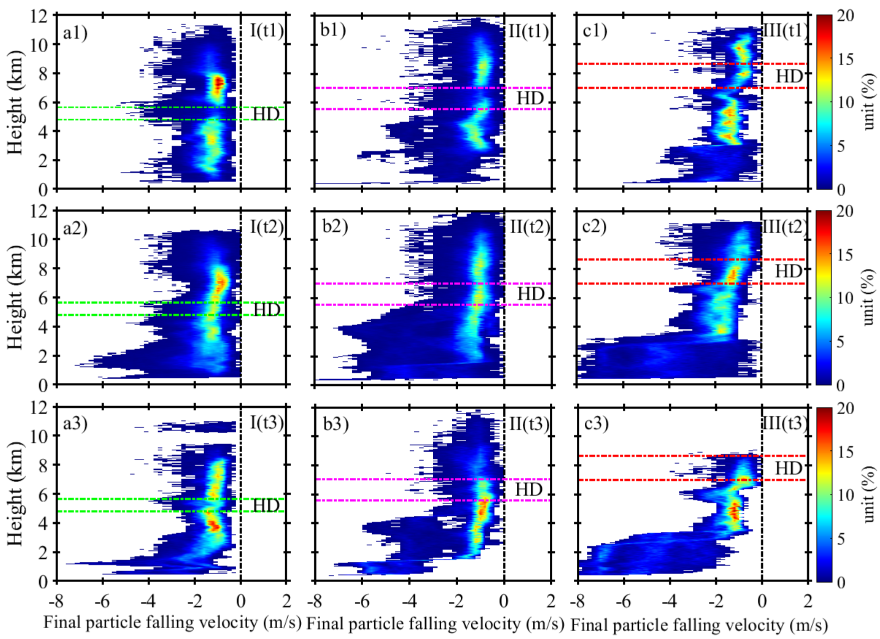

Figure 10 The CFAD of the final particle falling velocity in three types of seeder-feeder process before (t1), during (t2) and after (t3) seeding.

The final falling velocity of cloud particles is the net velocity of cloud particles after deducting the air flow velocity from the radial velocity of cloud particles, because the radial velocity is detected by radar in the vertical

https://doi.org/10.5194/egusphere-2023-2183
Preprint. Discussion started: 16 November 2023

direction, so the final falling velocity of cloud particles only represents the rising or sinking motion of cloud particles or zero velocity. As shown in Fig. 10, the probability density distribution with height of the final falling velocity in the three types of seeding and feeding clouds varies. In general, the final falling velocity of the three types mainly ranges from –0.5 ms^{-1} to –2 ms^{-1}, and the distribution of the final falling velocity during the seeding process (t2) and after the seeding process (t3) is wider than that before the seeding (t1). In the seeding process, the final falling velocity distribution is the widest (the maximum reaching to –6 ms^{-1} in the type II, and to –8 ms^{-1} in the type III). The sinking motion of cloud particles is located at the lower part of the feeding cloud after the seeding for the three types, which is likely to be caused by the seeding effect to increase the size of cloud particles under feeding clouds. Then, under the action of gravity, the descending speed of cloud particles increases, and even rainfall occurs (the type III). During the seeding period of the three types (Fig. 10a2, b2, c2), the descending velocity of cloud particles increased slightly with the descending height from the HD to the top of the feeding cloud, indicating that the size of seeders of the HD increased during the descending process and when they entered the upper part of the feeding cloud, which reflected the seeding effect of seeders. In the middle to lower part of the feeding cloud, the distribution of the final falling velocity is wide, which may be caused by the development of the feeding cloud itself, indicating that the seeding effect does not reach this region. After end of the seeding in the three types (Figs. 10a3, b3, c3), the final falling velocity of cloud particles increases in the middle and lower part of the feeding cloud, which could be understood as the delay of seeding effect to the lower part of the feeding cloud during the seeding period.

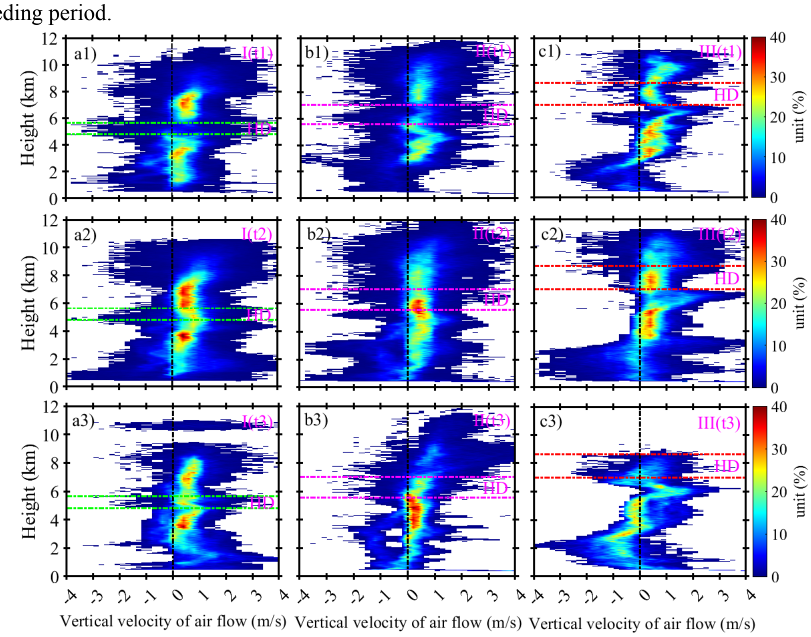

Figure 11 The CFAD of the vertical velocity of air flow in three types of seeder-feeder process before (t1), during (t2) and after (t3) seeding.

https://doi.org/10.5194/egusphere-2023-2183
Preprint. Discussion started: 16 November 2023

The vertical velocity distribution of airflow in clouds is a reflection of the dynamic structure of clouds. The airflow in stratiform clouds is usually slow, and the size and concentration of cloud particles change little. In convective clouds, there is a strong upward and downward movement of airflow, and cloud particles will experience cloud physical processes such as collision and growth, and the Bergeron effect under the airflow, so that large cloud particles will appear, and eventually rain or hail. Fig. 11 shows the distribution of probability density with height for the vertical velocity of airflow in the three types of seeding and feeding clouds. It shows that updraft and downdraft exist simultaneously in the cloud. The vertical velocity of airflow in the upper part of the seeding cloud is slightly larger than that in the lower part, which provides meteorological conditions for the growth of ice crystals in the seeding cloud, because the updraft transport water vapor needed for the growth of ice particles, and also increases the probability of collision between particles. The updraft velocity at the top of the feeding cloud is also slightly greater than that at the bottom. There is a slight difference between the three types, among which the type I and II are dominated by weak updrafts before, during and after seeding, and HD region is also dominated by weak updrafts, the updrafts are mainly distributed in the range of 0 ~1 ms^{-1} (probability density is greater than 20%). The probability density of strong or weak updraft (greater than 1 ms^{-1} or less than 0 ms^{-1}) is less than 20%. For the type III, before and during seeding, the distribution of probability density with height for the vertical velocity of airflow was similar to that of the type I and II, but after seeding, a large downdraft appeared in the HD region and in the middle and lower part of the feeding cloud. Fig. 10c3 also showed that the cloud particles in the lower part of the feeding cloud mainly moved down, while the echo showed that snow appeared at the bottom of the feeding cloud.

To understand the relationship between cloud particle variation and echo signal, the correlation coefficient between cloud particle falling velocity and corresponding reflectivity factor in each case of the three types during seeder-feeder period (t2) was calculated, and then averaged according to different categories. The height of average HD thickness in each type is taken as the basis, and the correlation coefficient profile and average reflectivity factor profile of the corresponding categories are obtained, as shown in Fig. 12. The cyan shaded area in the figure is the ESD layer. The average reflectivity factor profile in the figure shows that the height and thickness of the HD layer in the three types of seeder-feeder continuously increase from the type I to the type III, while the thickness of the ESD layer is on the contrary. The ESD in the type I is the thickest and it is the thinnest in the type III, which gives a conclusion that the HD height is high, and the ESD thickness is thin during seeding process. This process can be understood as that when HD is high, the cloud particles are small (that is, light particles in weight), so their falling speed is also small (see Fig. 10b2), so the depth of their falling into the top layer of the feeding cloud is also small.

https://doi.org/10.5194/egusphere-2023-2183
Preprint. Discussion started: 16 November 2023

On the contrary, when the cloud particles in HD are larger (i.e. heavier), the height of HD will be lower, so these particles will enter deeper into the feeding cloud, such as the type I.

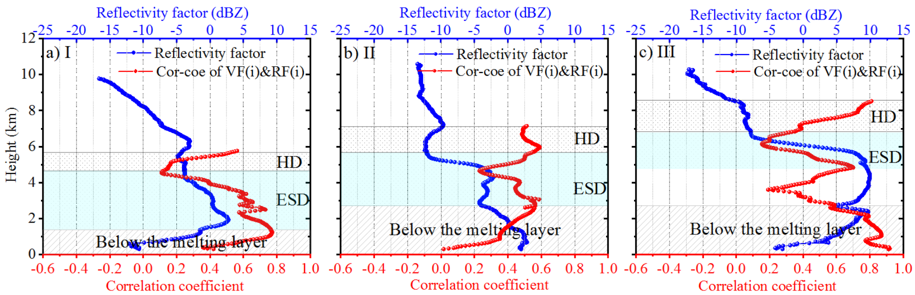

Figure 12 Autocorrelation coefficient profiles (red line) between cloud particle final falling velocity and reflectivity factor (blue line) during seeding (t2) for the type I (a), the type II (b) and the type III (c)

Fig. 12a shows more details in the feeding cloud such as the reflectivity factor increases with the decrease of the height and reaches the maximum value at 2 km, and the correlation coefficient also increases simultaneously with the reflectivity factor. That says close relationship between the reflectivity factor and the final falling velocity of cloud particles. The essence is that when the final falling velocity of cloud particles is large, it means that the cloud particles have a large mass and a large scale, then the reflectivity factor must be large. Fig. 10a2 also shows that there are a certain proportion of cloud particles in the middle and lower part of the ESD layer with a large sinking speed. However, at the bottom of feeding cloud, the reflectivity factor and the correlation coefficient decrease, indicating that there is basically no seeding effect at the bottom of feeding cloud during t2 period. The reflectivity factor increased rapidly but the correlation coefficient decreased rapidly at the top of feeding cloud in the second type. It is estimated that because the seeders in the HD region just fell into the top of the feeding cloud resulting in the number of cloud particles increased at the top, but these particles did not have time to grow, so although the echo reflectivity factor increased, the correlation coefficient decreased rapidly. When the seeders drop to a certain depth in the feeding cloud, the interaction between cloud particles such as collision occurs so that the correlation coefficient between cloud particle final velocity and echo reflectivity factor increases synchronously. Below the ESD region, the correlation coefficient decreases rapidly with the decrease of height, but the reflectivity factor continues to increase, which is probably caused by the high number of particles in the layer. In the third type, as the seeders enter the ESD region the reflectivity factor increases rapidly with the decrease of height together with the correlation coefficient increasing rapidly to the maximum. In the height from 5 km to 3.5 km, the correlation coefficient decreases obviously with the decrease of height, but the reflectivity factor maintains a large value (about 10 dBZ), which may indicate the high concentration of cloud particle in the height. In the lower part of the feeding

https://doi.org/10.5194/egusphere-2023-2183
Preprint. Discussion started: 16 November 2023

cloud, the reflectivity factor decreases with the decrease of the height, while the correlation coefficient increases, indicating that the particle final velocity in this height also decreases. It is likely that the cloud particles are so small that some of them evaporate, causing both the reflectivity factor and the final particle velocity to decrease simultaneously. In general, the depth of seeders injecting the feeding cloud is limited, and the lower and thinner the HD height is, the lower and thicker the ESD height is. Conversely, the higher the HD height, the higher and thinner the ESD height.

5. Conclusions

In this paper, the data of bilayer cloud in winter to the next spring detected by MWCR are analyzed, and the seeing-feeding phenomenon between the bilayer clouds in Xi 'an area is found. By defining the key parameters of the seeded cloud and the feeding cloud, such as the HD between the bilayer cloud and the ESD of the seeded cloud, the calculation method of the parametric probability density distribution with height and the analysis method of the correlation coefficient profile between the cloud particle final velocity and the reflectivity factor are adopted. The results show that: (1) During the 11 cases of bilayer cloud seeding and feeding, the seeding effect had a significant impact on the macro and micro parameters of the feeding cloud, which was mainly manifested in that the seeding effect caused a significant increase of the reflectivity factor and the falling velocity of cloud particles in the feeding cloud. Therefore, it was speculated that the seeding effect caused a significant increase in the particle size of the feeding cloud. (2) According to the distribution characteristics of ESD thickness and height, the seeder-feeder process of bilayer cloud can be divided into three categories, the type I has thin HD layer with low height, and its ESD layer is thick; The type III has thick HD layer with high height, its ESD layer thin; The thickness values of both HD and ESD of the type II lie between the type I and III. It can be inferred that the lower and thinner the HD height, the lower and thicker the ESD height; the reverse is also true. (3) According to the analysis results of 11 cases, the seeing-feeding process and related parameter distribution of a bilayer stratiform cloud are shown in Fig. 13, that is, during the evolution of a bilayer cloud, the phenomenon of cloud particles from the lower part of the upper-layer cloud seeding the lower-layer cloud will occur under appropriate weather background, that is, the distribution of air flow is unique with the height, and there is a relatively obvious updraft at the top of the seeding cloud. In the seeding layer (HD region and ESD region), the sinking motion of air flow and cloud particles is obvious, and when there is rainfall, the sinking motion at the bottom of the feeding cloud is stronger, and there is a small amount of down-flow region in the seeding cloud and the feeding cloud, but weak up-flow in the bilayer cloud. The seeding process can last up to 2 hours, but most seeding lasts for tens of minutes. Generally, seeding

https://doi.org/10.5194/egusphere-2023-2183
Preprint. Discussion started: 16 November 2023

takes place at –25°C to –10°C within the cloud. The seeding effect plays actions on the precipitation (rain or snow) intensity in the feeding cloud will be shown in the results of subsequent studies.

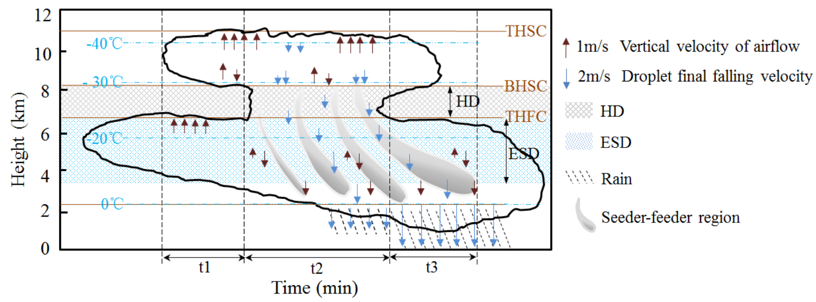

Figure 13 Schematic diagram of the natural seeder-feeder process and related parameter distribution.

Data availability

The data and codes related to this article are available upon request from the corresponding author.

Author contributions

Conceptualization: Huige Di
Investigation: Huige Di
Methodology: Huige Di
Software: Yun Yuan
Writing — original draft: Huige Di & Yun Yuan
Writing — review & editing: Huige Di
Supervision: Huige Di
Data collation: Yun Yuan

Competing interests

The authors declare that they have no conflicts of interest related to this work.

Acknowledgements

We express our gratitude to the Xi’an Meteorology Bureau of Shaanxi Province, Xi’an, Shehong Li, Shuicheng Bai, and Mei Cao for providing the relevant supporting data.

Financial support

This research was supported by the National Natural Science Foundation of China, the Innovative Research Group Project of the National Natural Science Foundation of China (Grant Nos. 42130612, 41627807), and the Ph.D. Innovation fund projects of Xi’an University of Technology (Fund No. 310-252072106).

References

1. Braham, R.R.: Cirrus Cloud Seeding as a Trigger for Storm Development, J. Atmos. Sci, 24, 311–312, https://doi.org/10.1175/1520-0469(1967)024<0311:CCSAAT>2.0.CO;2, 1967.
2. Cheng, C., and Yi, F.: Falling Mixed-Phase Ice Virga and their Liquid Parent Cloud Layers as Observed by Ground-Based Lidars, Remote Sens, 12, 2094, https://doi.org/10.3390/rs12132094, 2020.
3. Choularton, T.W., and Perry, S.J.: A model of the orographic enhancement of snowfall by the seeder-feeder mechanism, Quart. J.

https://doi.org/10.5194/egusphere-2023-2183
Preprint. Discussion started: 16 November 2023

R. Met. Soc, 112, 335-345, https://doi.org/10.1002/qj.49711247204, 1986.

4. Di, H., Yuan, Y., Yan, Q., Xin, W., Li, S., Wang, J., Wang, Y., Zhang, L., and Hua, D.: Determination of atmospheric column condensate using active and passive remote sensing technology, Atmos. Meas. Tech, 15, 3555–3567, https://doi.org/10.5194/amt-15-3555-2022, 2022.
5. Dong, X., Zhao, C., Huang, Z., Mai, R., Lv, F., Xue, X., Zhang, X., Hou, S., Yang, Y., Yang, Y., and Sun, Y.: Increase of precipitation by cloud seeding observed from a case study in November 2020 over Shijiazhuang, China, Atmos. Res, 262, 105766, https://doi.org/10.1016/j.atmosres.2021.105766, 2021.
6. Doviak, R. J., Zrnic, D. S., and Schotland, R. M.: Doppler radar and weather observations, Appl Optics, 33, 4531, 1994.
7. Fernández-González, S., Valero, F., Sánchez, J. L., Gascón, E., López, L., García-Ortega, E., and Merino, A.: Analysis of a seeder-feeder and freezing drizzle event, J. Geo-phys. Res. Atmos, 120, 3984–3999, https://doi.org/10.1002/2014jd022916, 2015.
8. French, J.R., Friedrich, K., Tessendorf, S.A., Rauber, R.M., Geerts, B., Rasmussen, R.M., Xue, L., Kunkel, M.L., and Blestrud, D.R.: Precipitation formation from orographic cloud seeding. P, Natl. Acad. Sci. Usa, 115, 1168–1173, https://doi.org/10.1073/pnas.1716995115, 2018.
9. Geerts, B., Pokharel, B., and Kristovich, D.A.R.: Blowing Snow as a Natural Glaciogenic Cloud Seeding Mechanism, Mon. Weather. Rev, 143, 5017–5033, https://doi.org/10.1175/MWR-D-15-0241.1, 2015.
10. Görsdorf, U., Lehmann, V., Bauer-Pfundstein, M., Peters, G., Vavriv, D., Vinogradov, V., and Volkov, V.: A 35-GHz Polarimetric Doppler Radar for Long-Term Observations of Cloud Parameters—Description of System and Data Processing, J. Atmos. Ocean. Technol, 32, 675–690, https://doi.org/10.1175/jtech-d-14-00066.1, 2015.
11. Hall, W.D., and Pruppacher, H.R.: The Survival of Ice Particles Falling from Cirrus Clouds in Subsaturated Air, J. Atmos. Sci, 33, 1995–2006, https://doi.org/10.1175/1520-0469(1976)033<1995:tsoipf>2.0.co;2, 1976.
12. He, Y., Liu, F., Yin, Z., Zhang, Y., Zhan, Y., and Yi, F.: Horizontally oriented ice crystals observed by the synergy of zenith- and slant-pointed polarization lidar over Wuhan (30.5°N, 114.4°E), China, J. Quant. Spectrosc. Ra, 268, 107626, https://doi.org/10.1016/j.jqsrt.2021.107626, 2021.
13. He, Y., Yi, F., Liu, F., Yin, Z., Yi, Y., Zhou, J., Yu, C., and Zhang, Y.: Natural seeder-feeder process originating from mixed-phase clouds observed with polarization lidar and radiosonde at a mid-latitude plain site, J. Geo-phys. Res. Atmos, 127, e2021JD036094, https://doi.org/10.1029/2021JD036094, 2022.
14. Heymsfield, A.J., Schmitt, C., Bansemer, A.: Ice Cloud Particle Size Distributions and Pressure-Dependent Terminal Velocities from In Situ Observations at Temperatures from 0° to −86°C, J. Atmos. Sci, 70, 4123–4154, https://doi.org/10.1175/jas-d-12-0124.1, 2013.
15. Hill, F. F., Browning, K. A., and Bader, M. J.: Radar and Raingauge Observations of Orographic Rain over South Wales, Q. J. Roy. Meteor. Soc, 107, 643–670, https://doi.org/10.1002/qj.49710745312, 2007.
16. Hong, Y.: Research Progress of Stratiform Cloud Structure and Precipitation Mechanism and Discussion on Artificial Precipitation Problems, Clim. Environ. Res, 17, 937-950, https://doi.org/10.3878/j.issn.1006-9585.2012.06.31, 2012.
17. Hou, T., Lei, H., and Hu, Z.: A comparative study of the microstructure and precipitation mechanisms for two stratiform clouds in China, Atmospheric Research, 96, 447–460, https://doi.org/10.1016/j.atmosres.2010.02.004, 2010.
18. Houghton, H. G.: On the Physics of Clouds and Precipitation, in: Compendium of Meteorology: Prepared under the Direction of the Committee on the Compendium of Meteorology, edited by: Byers, H. R., Landsberg, H. E., Wexler, H., Haurwitz, B., Spilhaus, A. F., Willett, H. C., Houghton, H. G., and Malone, T. F., American Meteorological Society, Boston, MA, 165–181, https://doi.org/10.1007/978-1-940033-70-9_14, 1951.
19. Kollias, P., Albrecht, B. A., Lhermitte, R., and Savtchenko, A.: Radar observations of updrafts, downdrafts, and turbulence in fair-weather cumuli, J. Atmos. Sci, 58, 1750-1766, https://doi.org/10.1175/1520-0469(2001)058%3C1750:ROOUDA%3E2.0.CO;2, 2001.
20. Kollias, P., Albrecht, B.A., Marks, F.: Why Mie? Accurate observations of vertical air velocities and raindrops using a cloud radar, Bull. Amer. Meteor. Soc, 83, 1471–1483, https://doi.org/10.1175/bams-83-10-1471, 2002.

21. Kollias, P., Rémillard, J., Luke, E., Szyrmer, W.: Cloud radar Doppler spectra in drizzling stratiform clouds: 1. Forward modeling and remote sensing applications, J. Geophys. Res, 116, D13201, https://doi.org/10.1029/2010JD015237, 2011.
22. Korolev, A. and Isaac, G.: Phase transformation of mixed-phase clouds, Q J Roy Meteor Soc, 129, 19–38, https://doi.org/10.1256/qj.01.203, 2003.
23. Korolev, A. V., Isaac, G. A., and Hallett, J.: Ice particle habits in Arctic clouds, Geophysical Research Letters, 26, 1299–1302, https://doi.org/10.1029/1999GL900232, 1999.
24. Korolev, A. V., Isaac, G. A., Cober, S. G., Strapp, J. W., and Hallett, J.: Microphysical characterization of mixed-phase clouds, Q J Roy Meteor Soc, 129, 39–65, https://doi.org/10.1256/qj.01.204, 2003.
25. Liu, L., Ding, H., Dong, X., Cao, J., and Su, T.: Applications of QC and Merged Doppler Spectral Density Data from Ka-Band Cloud Radar to Microphysics Retrieval and Comparison with Airplane in Situ Observation, Remote. Sens, 11, 1595, https://doi.org/10.3390/rs11131595, 2019.
26. Locatelli, J. D., Hobbs, P. V., and Biswas, K. R.: Precipitation from Stratocumulus Clouds Affected by Fallstreaks and Artificial Seeding, J. Clim. Appl. Meteorol., 22, 1393–1403, https://doi.org/10.1175/1520-0450(1983)022<1393:PFSCAB>2.0.CO;2, 1983.
27. Lowenthal, D.H., Hallar, A.G., David, R.O., Mccubbin, I.B., and Mace, G.G.: Mixed Phase Orographic Cloud Microphysics during StormVEx and IFRACS, Atmos. Chem. Phys, 19, 5387–5401, https://doi.org/10.5194/acp-19-5387-2019, 2019.
28. Luke, E. P., and Kollias, P.: Separating Cloud and Drizzle Radar Moments during Precipitation Onset Using Doppler Spectra, J. Atmos. Ocean. Technol, 30, 1656–1671, https://doi.org/10.1175/jtech-d-11-00195.1, 2013.
29. Myagkov, A., Seifert, P., Wandinger, U., Bühl, Johannes., Engelmann, R.: Relationship between temperature and apparent shape of pristine ice crystalsderived from polarimetric cloud radar observations during the accept campaign, Atmos. Meas. Tech, 9, 3739-3754, https://doi.org/10.5194/amt-9-3739-2016, 2016.
30. Proske, U., Bessenbacher, V., Dedekind, Z., Lohmann, U., and Neubauer, D.: How frequent is natural cloud seeding from ice cloud layers ($< -35^{\circ}$C) over Switzerland?, Atmos. Chem. Phys, 21, 5195–5216, https://doi.org/10.5194/acp-21-5195-2021, 2021.
31. Purdy, J. C., Austin, G. L., Seed, A. W., and Cluckie, I. D.: Radar evidence of orographic enhancement due to the seeder feeder mechanism, Meteorol. Appl, 12, 199–206, https://doi.org/10.1017/S1350482705001672, 2005.
32. Ramelli, F., Henneberger, J., David, R. O., Bühl, J., Radenz, M., Seifert, P., Wieder, J., Lauber, A., Pasqier, J. T., Engelmann, R., Mignani, C., Hervo, M., and Lohmann, U.: Microphysical investigation of the seeder and feeder region of an Alpine mixed-phase cloud, Atmos. Chem. Phys, 21, 6681-6706, https://doi.org/10.5194/acp-2020-772, 2021.
33. Ramelli, F., Henneberger, J., David, R.O., Lauber, A., Pasquier, J.T., Wieder, J., Bühl, J., Seifert, P., Engelmann, R., Hervo, M., and Lohmann, U.: Influence of low-level blocking and turbulence on the microphysics of a mixed-phase cloud in an inner-Alpine valley, Atmos. Chem. Phys, 21, 5151–5172, https://doi.org/10.5194/acp-21-5151-2021, 2021.
34. Robichaud, A. J., and Austin, G. L.: On the Modelling of Warm Orographic Rain by the Seeder-Feeder Mechanism, Q. J. Roy. Meteor. Soc, 114, 967–988, https://doi.org/10.1002/qj.49711448207, 1988.
35. Seifert, P., Ansmann, A., Mattis, I., Althausen, D., Tesche, M., Wandinger, Ulla., Muller, D., and Pérez, C.: Lidar-based profiling of the tropospheric cloud-ice distribution to study the seeder-feeder mechanism and the role of Saharan dust as ice nuclei, In: Proceedings of the 8th International Symposium on Tropospheric Profiling, Bergen, Norway, 2014.
36. Shupe, M. D., Kollias, P., Persson, P. O. G., and McFarquhar, G. M.: Vertical motions in Arctic mixed-phase stratiform clouds, J. Atmos. Sci, 65, 1304-1322, https://doi.org/10.1175/2007JAS2479.1, 2008.
37. Shupe, M. D., Uttal, T., and Matrosov, S. Y.: Arctic Cloud Microphysics Retrievals from Surface-Based Remote Sensors at SHEBA, J. Appl. Meteorol, 44, 1544–1562, https://doi.org/10.1175/jam2297.1, 2005.
38. Vassel, M., Ickes, L., Maturilli, M., and Hoose, C.: Classification of Arctic multilayer clouds using radiosonde and radar data in Svalbard, Atmos. Chem. Phys, 19, 5111–5126, https://doi.org/10.5194/acp-19-5111-2019, 2019.
39. Wang, H., Zhang, H., Wang, W., Wang, J., Li, Y., and Wang, S.: Microphysical characteristics of precipitation in multi-source mixed clouds, DQKX, 46, 886–902, https://doi.org/10.3878/j.issn.1006-9895.2107.21043, 2022.
40. Wang, Y., Kong, R., Cai, M., Zhou, Y., Song, C., Liu, S., Li, Q., Chen, H., and Zhao, C.: High small ice concentration in

https://doi.org/10.5194/egusphere-2023-2183
Preprint. Discussion started: 16 November 2023

stratiform clouds over Eastern China based on aircraft observations: Habit properties and potential roles of secondary ice production, Atmos Res, 281, 106495, https://doi.org/10.1016/j.atmosres.2022.106495, 2023.

41. Wei, T., Xia, H., Hu, J., Wang, C., Shangguan, M., Wang, L., Jia, M., and Dou, X.: Simultaneous wind and rainfall detection by power spectrum analysis using a VAD scanning coherent Doppler lidar, Opt Express, 27, 31235, https://doi.org/10.1364/OE.27.031235, 2019.
42. Yan-Chao, H. and Fei-Fei, Z.: A Numerical Simulation Study of Precipitation Formation Mechanism of “Seeding-Feeding” Cloud System, dqkx, 29, 885–896, https://doi.org/10.3878/j.issn.1006-9895.2005.06.05, 2005.
43. Yan-Chao, H. and Fei-Fei, Z.: The Study of Evaluation of Potential of Artificial Precipitation Enhancement in Stratiform Cloud System, dqkx, 30, 913–926, https://doi.org/10.3878/j.issn.1006-9895.2006.05.20, 2006.
44. Yu, G., Verlinde, J., Clothiaux, E. E., and Chen, Y.-S.: Mixed-phase cloud phase partitioning using millimeter wavelength cloud radar Doppler velocity spectra, J. Geophys. Res. Atmos., 119, 7556–7576, https://doi.org/10.1002/2013JD021182, 2014.
45. Yuan, Y., Di, H., Liu, Y., Cheng, D., Chen, N., Yan, Q., and Hua, D.: Confidence and Error Analyses of the Radiosonde and Ka-Wavelength Cloud Radar for Detecting the Cloud Vertical Structure, Remote. Sens, 14, 4462, https://doi.org/10.3390/rs14184462, 2022.
46. Yuan, Y., Di, H., Liu, Y., Yang, T., Li, Q., Yan, Q., Xin, W., Li, S., and Hua, D.: Detection and analysis of cloud boundary in Xi'an, China, employing 35 GHz cloud radar aided by 1064 nm lidar, Atmos. Meas. Tech, 15, 4989-5006, https://doi.org/10.5194/amt-15-4989-2022, 2022.
47. Yuan, Y., Di, H., Wang, K., Bai, S., Yan, Q., Cao, M., Zhang, Y., Wang, Y., and Hua, D.: Fine recognition technology of cloud phase based on multidimensional data, Acta Opt. Sin, 42, 268-278, https://doi.org/10.3788/AOS202242.1228002, 2022.